Linking Observed Seismicity to Crustal Structure in the New Madrid Seismic Zone Using Gravity and Magnetic Modeling

by

Caleb Myers Eldridge

A thesis submitted to the Graduate Faculty of
Auburn University
in partial fulfillment of the
requirements for the Degree of
Master of Science

Auburn, Alabama
August 3, 2019

Approved by

Dr. Lorraine W. Wolf, Chair, Professor, Department of Geosciences
Dr. Mark Steltenpohl, Professor, Department of Geosciences
Dr. Ming-Kuo Lee, Professor, Department of Geosciences

Abstract

The New Madrid Seismic Zone in the Central United States is a highly active seismic zone. Research has focused on the subsurface structure and history of development in order to gain better insight into the cause of these intraplate earthquakes. Geophysical and geologic data were incorporated to create crustal models along a transect in the New Madrid Seismic Zone (NMSZ) to gain a better understanding of the deep structure of the region and its relationship to potential sources of prehistoric earthquakes. A comprehensive database consisting of LiDAR data, geologic data, well-log information, and locations of liquefaction deposits was assembled in ESRI ArcGIS™ to provide a framework for interpreting the gravity and magnetic data.

Potential field analyses identified prominent features in the region that occur in close proximity to the locations of earthquakes. Large anomalies are interpreted as igneous intrusions that vary laterally in composition. Prominent lineations in the data highlight the rift margins and Reelfoot fault. For this study, two transects were chosen to cross key features identified from potential field observations. The models indicate a large mafic body beneath the region that shows a spatial correlation with areas of high seismicity, suggesting that this body is controlling the high seismicity in the region.

Acknowledgments

I would especially like to express my gratitude for my thesis advisor, Dr. Lorraine Wolf, who has been a tremendous support throughout my education here at Auburn. I am thankful for her willingness to take me on as an undergraduate who was just beginning to explore a future as a geologist at Auburn. Her constant guidance and expertise has shaped me tremendously and I know that I will be able to have a great career moving forward because of her support. I also would like to thank the other members of my committee. Dr. Ming-Kuo Lee was my undergraduate advisor while at Auburn, and his guidance helped me to pursue classes that would be of the best benefit to me. He also was an incredible teacher. Dr. Mark Steltenpohl was the first person that I spoke to when I was deciding to pursue geology, and our conversation convinced me that geology was the right path for me. Thank you all for your serving as members of my committee.

The rest of the faculty and staff in the Department of Geosciences at Auburn University is also deserving of thanks. Each and every member past and present has served a pivotal role in my tenure here at Auburn University, and for that I am thankful.

I also want to extend thanks to those who have helped at various stages of this project. Thank you to Dr. Kevin Mickus for providing gravity data used in this study, and thank you to Dr. Heather DeShon for providing the relocated earthquake catalogue. I also want to thank any of those not mentioned for all of the support provided to me.

Last but not least, thank you to my family. My parents Darrell and Christy Eldridge for loving and supporting me through my education and sister Anna Grace for always loving me. I especially am thankful for my wife Caroline. Without your love, kindness, and patience, as well as always listening to me talk about my work which I know you had no understanding of, I would never have gotten to where I am today. Thank you so much.

Table of Contents

List of Figures

List of Tables

List of Abbreviations

AF	Axial Fault
CGL	Commerce Geophysical Lineament
ERM	Eastern Rift Margin
LiDAR	Light Detection and Ranging
MGL	Missouri Gravity Low
NMSZ	New Madrid Seismic Zone
RF	Reelfoot Fault
SVD	Second Vertical Derivative
TDR	Tilt Derivative Filter
TFA	Total Field Anomaly

Introduction

The New Madrid Seismic Zone (NMSZ), located in parts of Tennessee, Arkansas, and Missouri, is the most seismically active fault zone east of the Rocky Mountains (Figure 1). Although most of the earthquakes are small and not always felt by humans, the NMSZ has hosted large earthquakes in the historic and prehistoric past. In 1811-1812, a series of three large earthquakes (M > 7) resulted in massive damage and widespread soil liquefaction. Such earthquakes, were they to happen today, would result in widespread damage to cities and towns along the Mississippi River valley, including Memphis, Tennessee, and St. Louis, Missouri. Analyses of earthquake-induced liquefaction deposits, such as sand blows and sand fissures, suggest that events similar in size to those of 1811-1812 have occurred in the past. These studies suggest a recurrence interval of ~ 500 years for the last 1200 years (Tuttle et al., 2002; 2019). These findings underscore the importance of identifying potential seismic sources in the region and understanding their geologic history.

The NMSZ is located in the stable interior of North America and according to estimates made from global positioning systems, the region lacks significant strain accumulations needed to generate large earthquakes (Newman et al., 1999). The large magnitude of the 1811-1812 events as well as the prehistoric events pose an enigma to researchers trying to understand the underlying cause for such seemingly unusual events. As technology has become more advanced, so has the available data, which have allowed for a better understanding of the nature of the earthquakes in this region. Geophysical studies have been useful in creating models to explain the geologic history and subsurface structures responsible for concentrating stress that

could lead to earthquakes. This study seeks to address questions about the relationship of seismicity to crustal structure and tectonic development of the NMSZ. The study uses gravity and magnetic data to construct models of the deep structure underlying areas of high seismicity and to investigate the possible relationship of these structures to neotectonic activity.

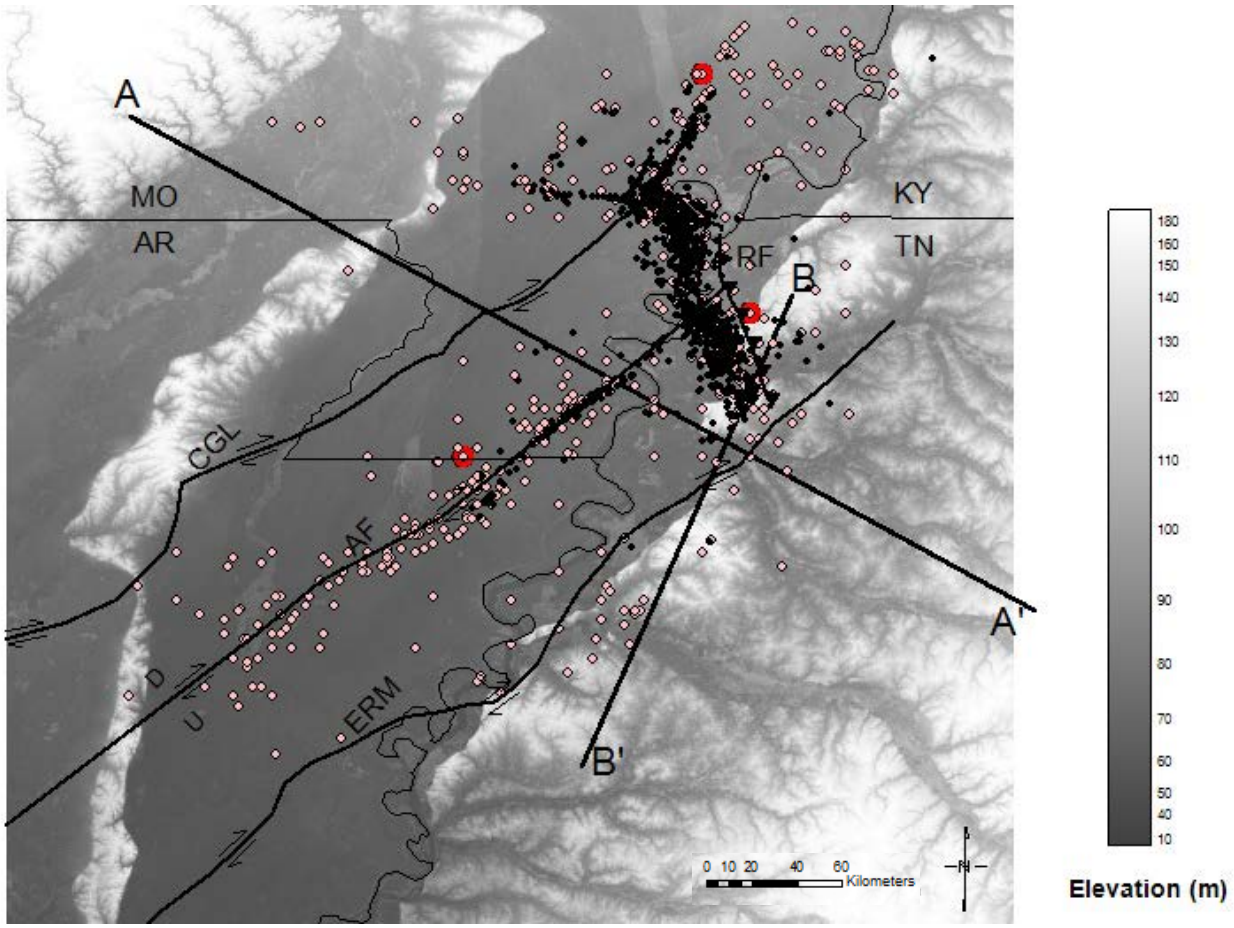

Fig. 1. Digital elevation map of the New Madrid Seismic Zone showing locations of profiles (A-A′; B-B′) modeled in this study. Black dots show relocated epicenters recorded by the Cooperative New Madrid Seismic Network from 2000 to 2007 and the 1989-1992 Portable Array Network and Data Acquisition deployment (modified from Dunn et al., 2013). Pink dots show earthquake epicenters (1811-2008, $M \geq 2.2$; from CEUS-SSC database). Red dots show the estimated epicentral locations of the 1811-1812 $M > 7$ earthquakes. Abbreviations are CGL=Commerce Geophysical Lineament; AF=Axial Fault; ERM=Eastern Rift Margin and RF= Reelfoot Fault (modified from Csontos and Van Arsdale, 2008). Sense of motion is indicated.

Geologic Setting / Tectonic History

The NMSZ was formed through tectonic activity that includes extension, compression, uplift, subsidence, sedimentary deposition, and igneous intrusions. Analyses of gravity, aeromagnetic and geologic data suggest that the embayment is part of a late Precambrian rift. Ervin and McGinnis (1975) constructed a general crustal model based on gravity and seismic data to explain the structure beneath the NMSZ as a failed rift zone. They suggest that the rift formed during late Precambrian time, uplifting the embayment and emplacing a low-density mantle material at the base of the crust. Faults associated with the rifting are still active today.

Subsidence began in the Paleozoic during the Taconic orogeny and continued into the Acadian orogeny (Braile et al., 1986) (Figure 2), creating compressive stress on the rift zone. During this time, carbonate and clastic Paleozoic rocks of marine origin were deposited above Precambrian granites and dioritic gneiss, as the Reelfoot Basin was being formed (Cushing et al., 1964; Ervin and McGinnis 1975; Mooney et al., 1983). Following deposition and the formation of the inner seaway, Mesozoic mafic to ultramafic rocks were intruded into the basin. Drill-hole data indicate these intrusive rocks are syenitic in composition (Hildenbrand, 1985). Igneous intrusions were accompanied by reactivation and uplift of the embayment (Hildenbrand, 1985).

A proposed model for the reactivation and uplift of the embayment is the passage of the Bermuda hot spot (Cox and Van Arsdale, 2002) (Figure 3). As the hot spot passed beneath the rift during the Cretaceous, the lithosphere was uplifted and eroded. Preexisting faults from the formation of the rift then served as conduits for Cretaceous igneous intrusions. Once the hot spot passed, the area subsided and was followed by deposition of the Upper Cretaceous McNairy

Formation directly above the marine Paleozoic rocks and igneous intrusions (Hildenbrand and Hendricks, 1995; Csontos and Van Arsdale, 2008). Deposition of clastic sediments into the Reelfoot basin continued throughout the Paleocene and Eocene, forming the major units of the Porters Creek Clay, Wilcox Group and Claiborne Group. These units were topped with unconsolidated Quaternary alluvium deposited by the Mississippi River and its tributaries, which continues today (Figure 4).

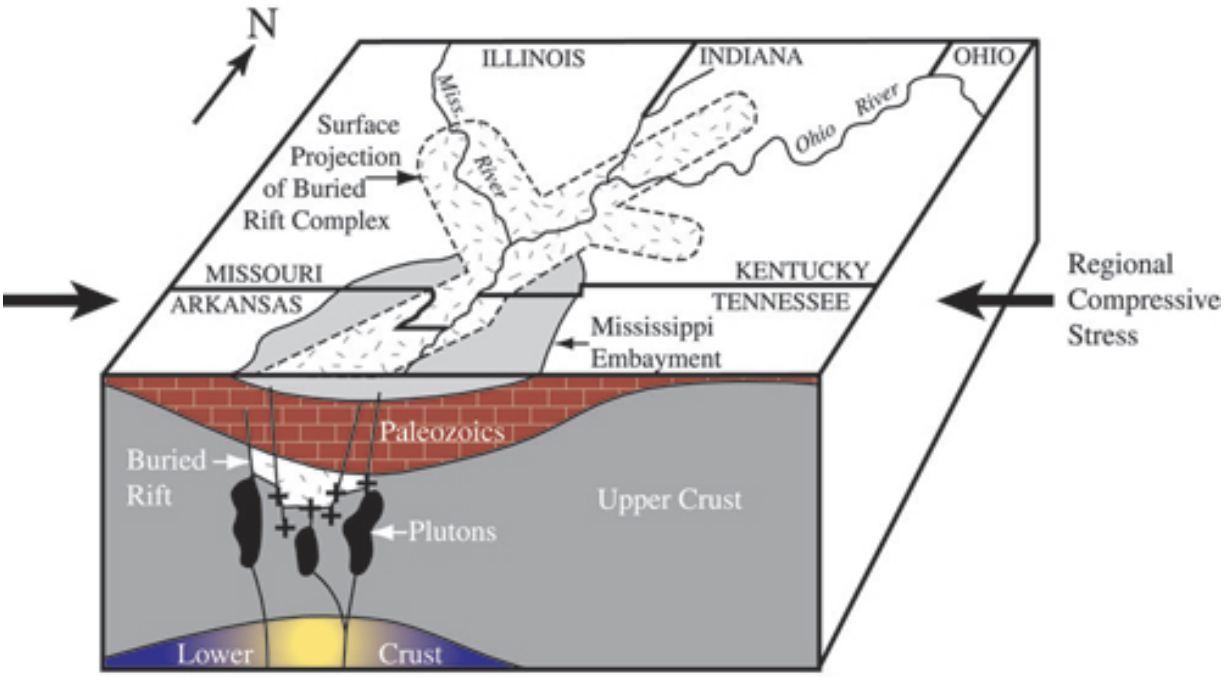

Fig 2. Model illustrating the tectonic setting of the Reelfoot Rift system thought to be responsible for seismicity in the NMSZ (from Braile et al., 1986).

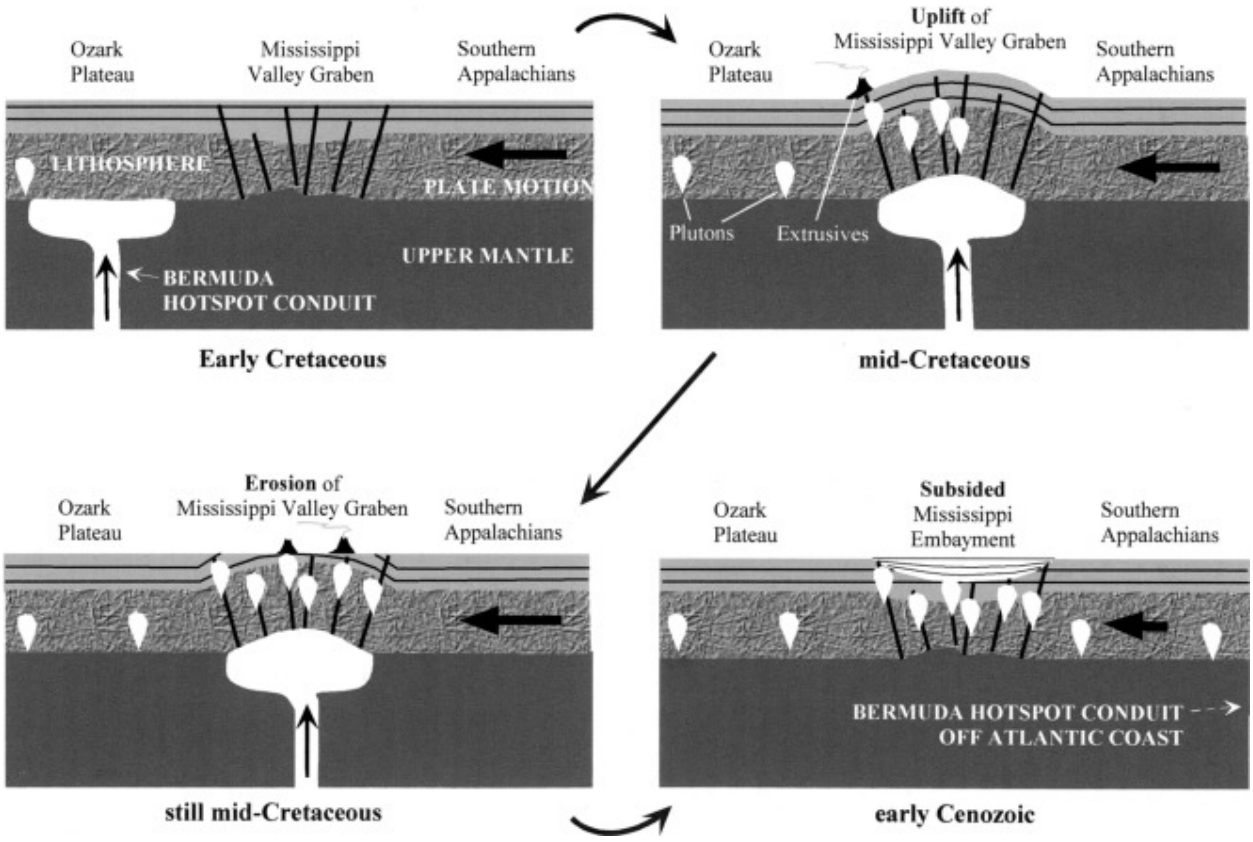

Fig. 3. Illustration showing the Cretaceous development of the NMSZ due to the passage of the Bermuda Hot spot. The white bodies show the Mesozoic intrusions that move up the Precambrian faults (from Cox and Van Arsdale, 2002).

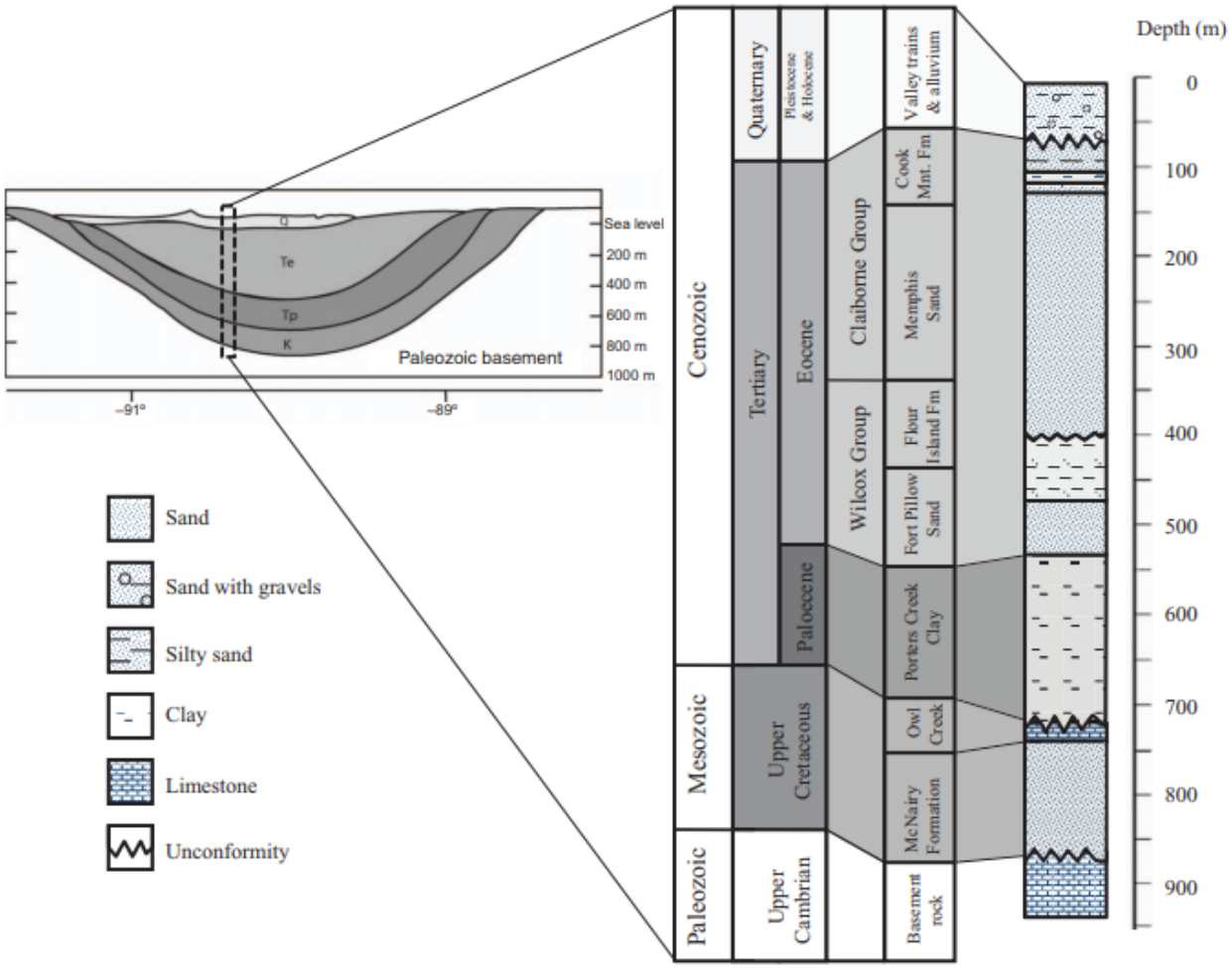

Fig. 4. Generalized cross section and stratigraphic column of the Mississippi Embayment (from Hardesty et al., 2010).

Previous Work

Much work has been done in the NMSZ to determine its overall structure and complex geologic history. Building on the conceptual model of Ervin and McGinnis (1975) for the development of a failed rift, Mooney et al. (1983) developed a more detailed crustal model for the embayment based on seismic refraction data (Figure 5). This model consists of five primary layers (from top to bottom): (1) unconsolidated Mesozoic and younger sediments (1.8 km/s), (2) Paleozoic carbonate and clastic sedimentary rocks (5.95 km/s), (3) a low-velocity layer of Early Paleozoic sediments (4.9 km/s), (4) a crystalline upper crust (6.6 km/s), and (5) a modified lower crust (7.3 km/s). Mooney et al. (1983) assert that their model of the embayment is consistent with the structure of other continental rifts in that it hosts a high-velocity layer, or "rift pillow," at the base of the crust. This high-velocity layer suggests that the lower crust has been modified by the injection of mantle material, which has in turn, depleted the upper mantle.

Analyses of gravity and magnetic data have added to the tectonic framework of the NMSZ. Hildenbrand (1985) and Hildenbrand and Hendricks (1995) used gravity data to suggest the presence of dense, shallow igneous intrusions and a high-density lower crust (Figure 6). Hildenbrand (1985) interpreted short-wavelength magnetic highs along the margins of the rift as shallow mafic or ultramafic dikes and sills, and long wavelength magnetic anomalies as prominent plutons. He postulated that the Covington pluton, which forms a well-defined magnetic high, likely varies laterally in composition, having a dense, highly magnetic core, but a lower susceptibility outer ring. Cross-sectional models derived from the gravity and magnetic

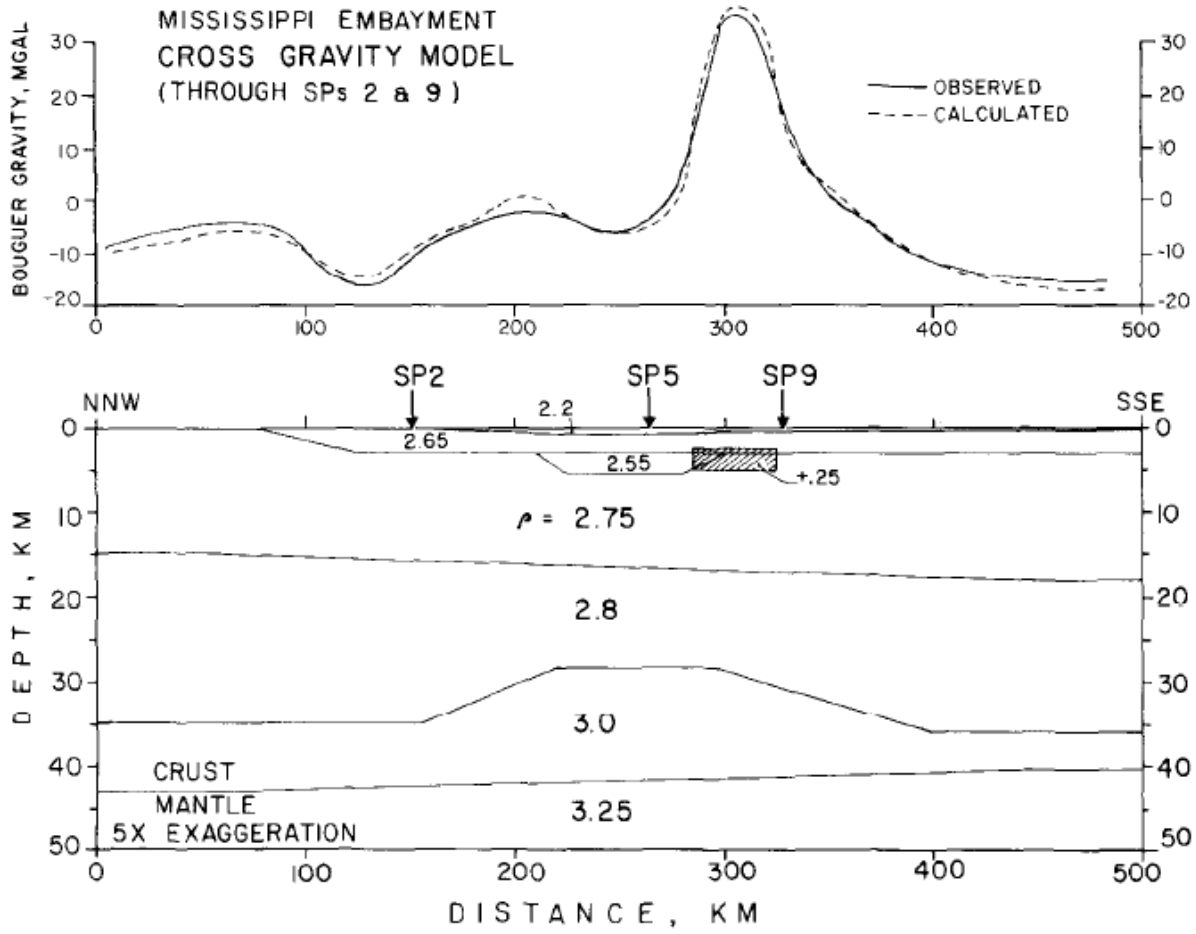

Fig. 5. Crustal model of the Mississippi Embayment proposed by Mooney et al. (1983). Densities are calculated from velocities of the seismic refraction model (see text for seismic model details). Two features of the model distinguish it from most continental crust: (1) a low-velocity/low density zone (2.55 kg/m^3) in the upper crust (Paleozoic layer) in the center of the model, and (2) a high-velocity/high-density (7.3 m/s; 3.25 kg/m^3) layer (rift pillow) in the lower crust.

data are consistent with earlier interpretations of a failed rift having a complex intrusive history (Hildenbrand, 1985).

More recent studies have focused on the Reelfoot fault and on the Pascola Arch. Rabak et al. (2011) proposed that the Pascola Arch formed around the same time as the Reelfoot fault. A spatial relationship between the magnetic anomaly formed by the Pascola Arch and earthquake epicenters supports this idea since the earthquakes are occurring within the intrusion causing the magnetic anomaly. This intrusion is shown to be heterogeneous in composition, with varying densities and susceptibilities, similar to the Covington Pluton as described by Hildenbrand (1985). A gravity model published by Liu et al. (2017) shows the existence of a mafic high-density upper crustal layer, which is rare for continental rifts but could explain the second phase of subsidence (Figure 7). This finding is consistent with a previous study by Pollitz et al. (2001), in which they propose that the stress concentration is due to a sinking mafic body in the lower crust. They note that this anomalous body is directly beneath the area with the highest seismicity the region: the axial fault, thrust faults along the northern margin, and right-lateral strike-slip faults along the eastern margin of the NMSZ.

Several studies attempted to link their interpretations of crustal structure to seismicity in the NMSZ. Ravat et al. (1987), using gravity and magnetic modeling in conjunction with observed seismicity, noted that most of the earthquakes in the NMSZ occur to the southeast of the Bloomfield pluton, one of the most prominent plutons in the NMSZ. They suggest that the presence of the pluton may be controlling the locations of the earthquakes. Langheim and Hildenbrand (1997) proposed that the Commerce Geophysical Lineament (CGL), a northeast-trending gravity and magnetic anomaly that extends for about 400 km along the western margin of the rift, is the result of focused igneous activity and is responsible for some of the observed

seismicity (Figure 1). Several anomalies seen in the potential field data appear to correlate with the locations of earthquakes activity, especially the intersection of the Reelfoot graben and the Missouri Batholith (Langheim and Hildenbrand, 1997). Others explained the concentration of earthquakes along the central axis of the graben as a crustal weak zone along the rift axis (Hildenbrand and Hendricks, 1995).

Csontos et al. (2008) used drill core data to construct contour maps of basement rocks to identify possible faults and the geometry of the fault planes associated with NMSZ seismicity. By creating surface maps of the contacts between the embayment units, they were able to construct a crustal cross-section from the rift pillow to ground surface. They concluded that many earthquakes appear to be aligned along the Precambrian fault planes of the Reelfoot Rift. Like previous workers, Csontos et al. (2008) interpreted the NMSZ as a right-lateral strike-slip fault zone with a left step-over restraining bend. They postulated that two of the major faults identified in the study, the Reelfoot North and Reelfoot South faults, are thrust faults (Csontos et al., 2008).

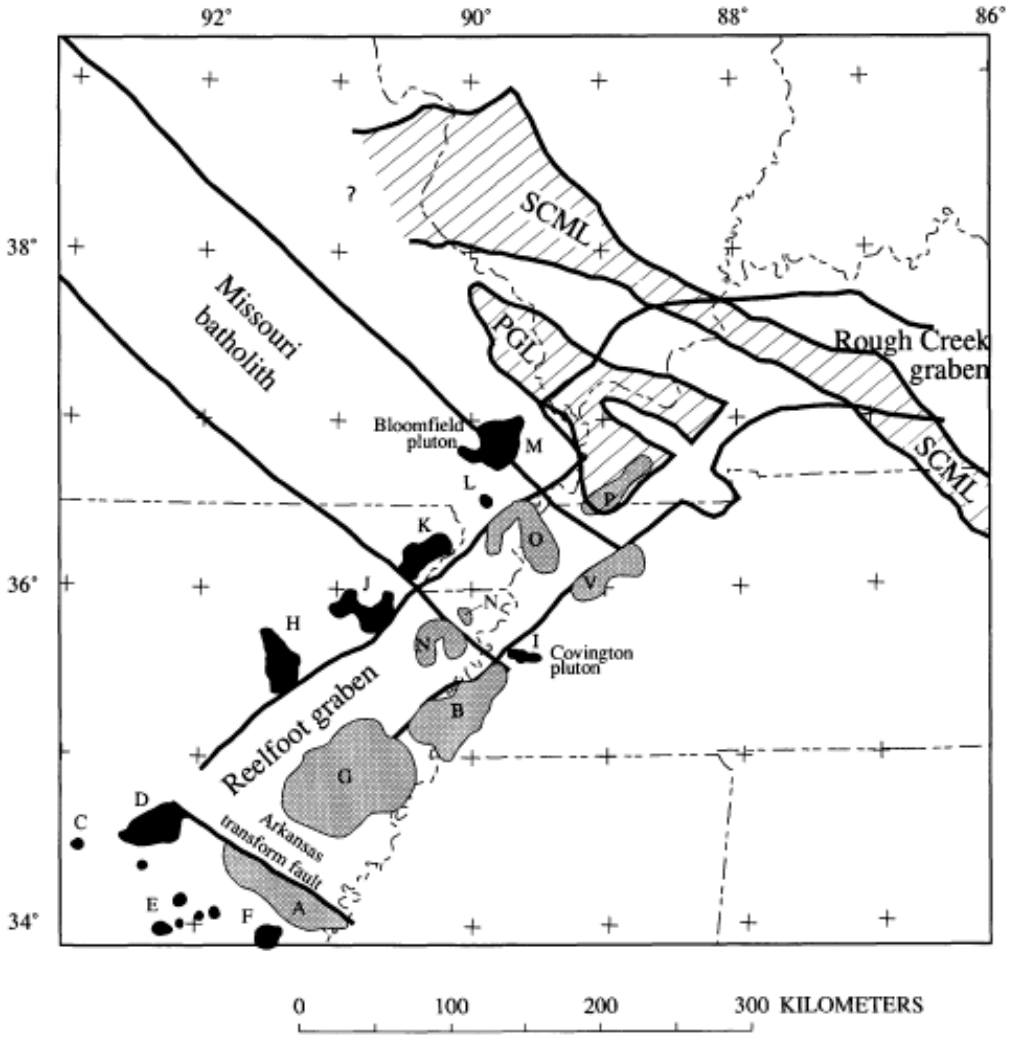

Fig. 6. Regional geophysical features indicated by Hildenbrand and Hendricks (1995). Dark and grey-shaded bodies represent intrusive complexes present in the NMSZ. Most of the intrusions are located along the margins of the rift zone, except for the Osceola igneous complex (N) and the Pascola (O). Other abbreviations as in Hildenbrand and Hendricks (1995).

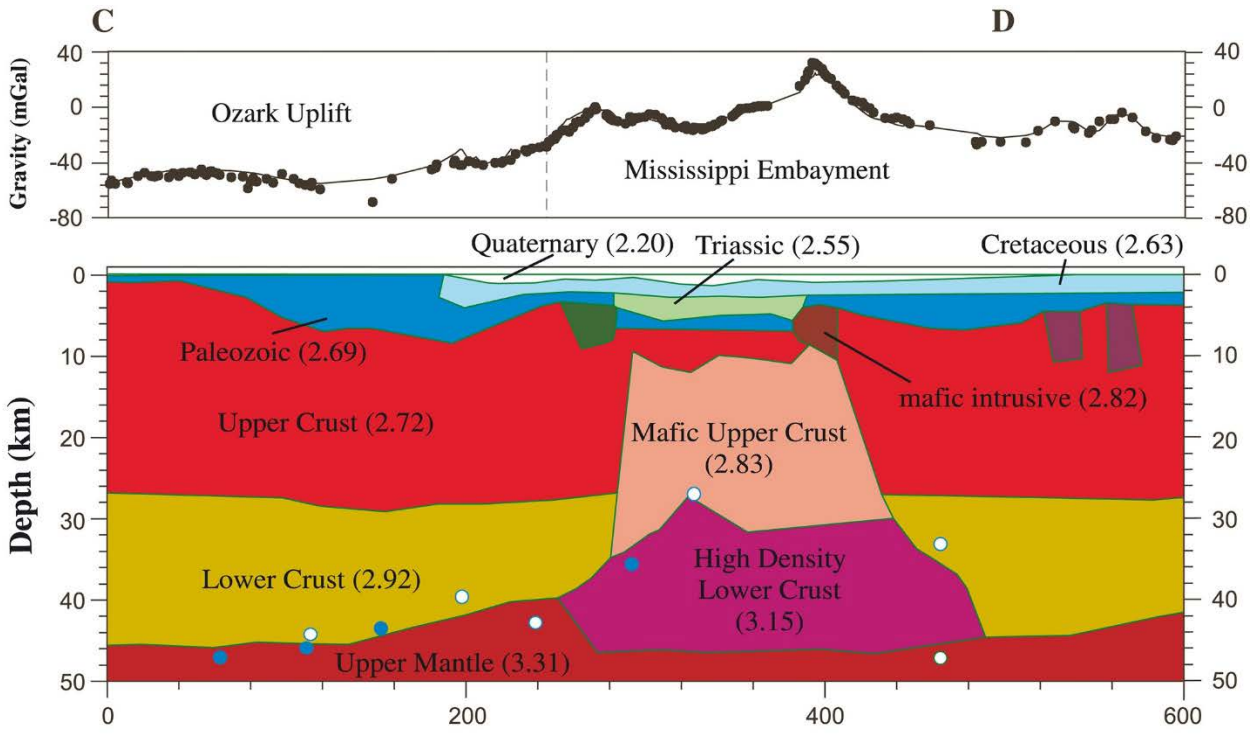

Fig. 7. Crustal model across the NMSZ (Liu et al., 2017). The model shows a mafic upper crustal intrusion believed to be responsible for the second phase of subsidence in the NMSZ. The density values served as a basis for the present study.

Methodology

This section is focused on the data collection and processing methods used in this study. The data collection consisted of compiling a database of light detection and ranging (LiDAR) data, geologic data, well-log information, locations of liquefaction deposits, and other supporting data into a geographic information system (GIS). Gravity and magnetic data were also obtained from various sources and compiled within Geosoft's Oasis Montaj™. Data processing included the analysis of gravity and magnetic anomaly maps and constructing 2.5 D crustal models along two transects that crossed several key tectonic features. Details of the data collection and data processing are described below.

GIS Database

Datasets were compiled into a database using ESRI ArcGIS™. These included aerial imagery from the U. S. Geological Survey; mapped locations of known or suspected basement faults (Csontos, 2008); geologic data, including rock units and liquefaction features; and information on earthquake locations and magnitudes from the Central and Eastern United States--Seismic Source Characterization for Nuclear Facilities (CEUS-SSC, 2015). A subset of relocated earthquakes was also included for this study (Dunn et al., 2013).

Gravity Data

The force of gravity varies on Earth's surface due to changes in densities of underlying rocks, latitude, elevation, and topography. To be accurate, several corrections to the data must

be applied in order to attribute the observed gravity to changes in varying rock composition and subsurface structures in earth's crust. These corrections are the Bouguer, free air, latitude, and terrain corrections. A database of gravity used for the study area consists of values from the U.S. Department of Defense, the U. S. Geological Survey, and data collected by Mickus and others (personal communication, 2018). For this study, a Bouguer reduction density of 2.67 g/cm^3 was assumed. Terrain corrections were not performed because topographic effects are considered negligible in the study area.

Magnetic Data

Earth's magnetic field varies due to the distribution of magnetic materials in the crust. Igneous and metamorphic rocks tend to contain more magnetic minerals than most sedimentary rocks, and thus produce stronger magnetic anomalies. High gradients can often correlate with fault zones or sharp lithologic contacts, where rocks of differing magnetic susceptibilities are juxtaposed. The aeromagnetic data used for this study is the total field anomaly (U.S. Geological Survey, 2002). The flight height was ~300 m (1000 ft), with a line spacing that was regridded to 1 km.

Data Processing

The gravity and magnetic datasets used in the study were processed and analyzed using Geosoft's Oasis Montaj™. This software is able to create digital grids of the datasets that can be processed using various filters and wavelength-separation techniques to aid in the interpretation of potential field anomalies. Cross-sections are created using the GM-SYS® profile extension within Oasis Montaj™. This software allows the user to create polygons whose depth, density,

and magnetic susceptibility can be adjusted to generate synthetic data values to match the observed geophysical data.

Gravity Data Processing

The gravity data were gridded using the minimum curvature method to create a complete Bouguer anomaly map for visual analysis (Figure 8). The minimum curvature method works by fitting a minimum curvature surface to the data points. It uses an iterative method to fit the data to the average values of points within a certain radius from a node point until the data reaches a satisfactory fit within the program's parameters (Resources GEOSOFT).

Gridded data were then used to create second vertical derivative (SVD) maps of the study region. The SVD filter uses the rate of change of the slope of the gridded gravity data. This technique is sensitive to shallow features, noise, and topography, and thus useful in clarifying the spatial dimensions of the source of the anomalies (Reynolds, 1997). Also used in the gravity processing was the tilt derivative filter (TDR) (described below).

Magnetic Data Processing

The total field anomaly data were gridded using a similar procedure to the gravity data in order to create a total field anomaly map (Figure 9). In addition to the total field anomaly, a TDR filter was used to determine spatial extent and edges of the causative bodies of observed anomalies in the data, following the method described in (Verduzco et al., 2004). The tilt angle of a magnetic anomaly is equivalent to local phase given by

$$\theta = \tan^{-1}\left(\frac{\frac{\partial A}{\partial z}}{\frac{\partial A}{\partial h}}\right), \qquad (1)$$

where the numerator and denominator are the vertical and horizontal derivatives of the anomaly (Blakely et al., 2016). Once the derivative filter is applied, the zero contour can be plotted, showing the mapped shape and approximate dimensions of the causative body (Blakely et al., 2016).

Gravity and Magnetic Profile Modeling

Gravity and magnetic profile modeling was completed using GM-SYS® 2.5D. Two transects extracted from the complete Bouguer anomaly grid and the total field magnetic anomaly grid were chosen for cross-sectional modeling (A-A′ and B-B′) (Figures 1, 8 and 9). Line A-A′ runs from west to east across the Reelfoot rift, and line B-B′ runs subparallel to the rift zone. The two intersect to form a tie line. Both lines cross key tectonic and geophysical features in the rift zone. Profile A-A′ crosses the CGL and the ERM, which are considered to represent the rift margins, and the central rift axis, along which the southeastern branch of seismicity is concentrated (Figure 1). Profile B-B′ crosses the Covington Pluton, which forms a pronounced anomaly in the potential field data. It also crosses the Reelfoot fault, which is coincident with a northwest-oriented line of earthquakes. Profile B-B′ forms a tie with Profile A-A′, which adds a constraint to the modeling. Both profiles cross extensive areas containing earthquake-induced liquefaction deposits. The liquefaction deposits are indicative of active seismic activity, and the goal in crossing these is to determine if there are unexposed faults related to the location and orientation of the deposits. Both profiles were oriented approximately perpendicular to the potential field gradient in an effort to reduce three-dimensional effects. The 2.5D algorithm assumes that the subsurface geology remains the same for some distance perpendicular to the profile.

The GM-SYS® software uses a forward-modeling procedure in which a theoretical curve for both gravity and magnetic values is calculated for an assumed geologic model. Polygons in the cross-sectional model are used to represent individual rock bodies or units in the subsurface. Horizontal layers are used to represent rock layers that extend the entire model length. For this study, initial density and magnetic susceptibility values were assigned based on rock type and composition, if known. Previously published models for other areas in the rift zone (Mooney et al., 1983; Hildenbrand, 1985; Liu et al., 2017) were also used to develop apriori structural models. Once the starting models were created, points were inserted to change the geometry of each unit or layer until an acceptable match between the observed data and the calculated (theoretical) data was achieved. The maximum misfit for error was 0.466 for the gravity data and 9.014 for the magnetic data. Adjustments to the densities and magnetic susceptibilities assigned to different geologic units were also be made in an effort to fit the observed data.

Results

Gravity and Magnetic Anomaly Maps

The Bouguer anomaly map (Figure 8) shows several gravity highs (> 10 mGal) (labeled **1** and **2**) believed to be associated with igneous intrusions, an interpretation consistent with previous work (Hildenbrand 1985; Liu et al., 2017). The circular gravity high to the north (labeled **1**) is the Bloomfield pluton, and the gravity high to the south (labeled **2**) is the Covington pluton. A gravity low, occupying a large portion of the central part of the Reelfoot rift, is bounded by gravity highs along the rift margins (CGL and ERM) and to the north of the northwest-trending Reelfoot fault. A broad gravity low (< 30 mGal) in the northwest section of the map is known as the Missouri gravity low (MGL).

In the total field anomaly map (Figure 9), the CGL and ERM appear as prominent northeast-trending lineaments, defined by high gradients of magnetic values separating the central part of the Reelfoot Rift from its margins. The Bloomfield pluton (**1**) is associated with a well-defined, circular magnetic high, while the Covington pluton (**2**) is less prominent in the data. The spatial distribution of the high magnetic anomalies suggests a lateral variation in composition of the intrusive bodies, likely due to fractionation of minerals during cooling or differing magmatic sources for different intrusive periods. Although seismicity associated with the northwest-trending Reelfoot fault correlates with a high, northwest-trending magnetic lineament, other bands of seismicity do not (e.g., the northeast-trending band of seismicity along the central rift axis). Two northeast bands of seismicity appear slightly deflected along the margins of the Bloomfield pluton; however, in other areas, the seismicity appears to cut through

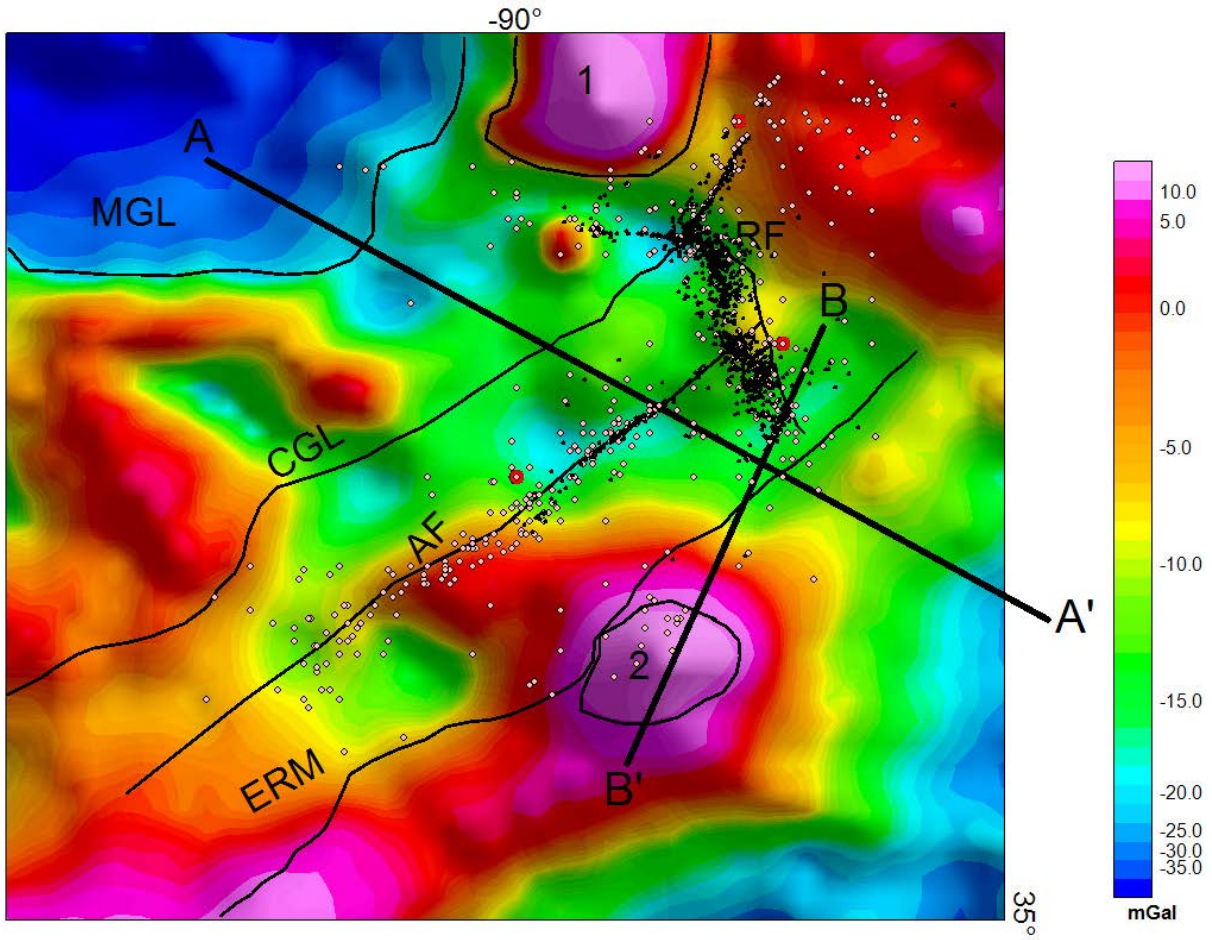

Fig. 8. Complete Bouguer gravity anomaly map created using a reduction density of 2.67 g/cm^3. Data from the Department of Defense, U. S. Geological Survey, and K. Mickus (pers. communication, 2018). The Missouri gravity low (MGL) is associated with the Missouri batholith. Prominent gravity highs are associated with the Bloomfield pluton (labeled 1) and the Covington pluton (labeled 2). Profiles A-A and B-B were chosen to cross the Commerce Geophysical Lineament (CGL), the Axial fault (AF), the Eastern Rift Margin (ERM), and the Reelfoot fault (RF). Pink dots show earthquake epicenters (1811-2008, $M \geq 2.2$; from CEUS-SSC database). Small black dots=relocated earthquake epicenters from Dunn et al. (2013).

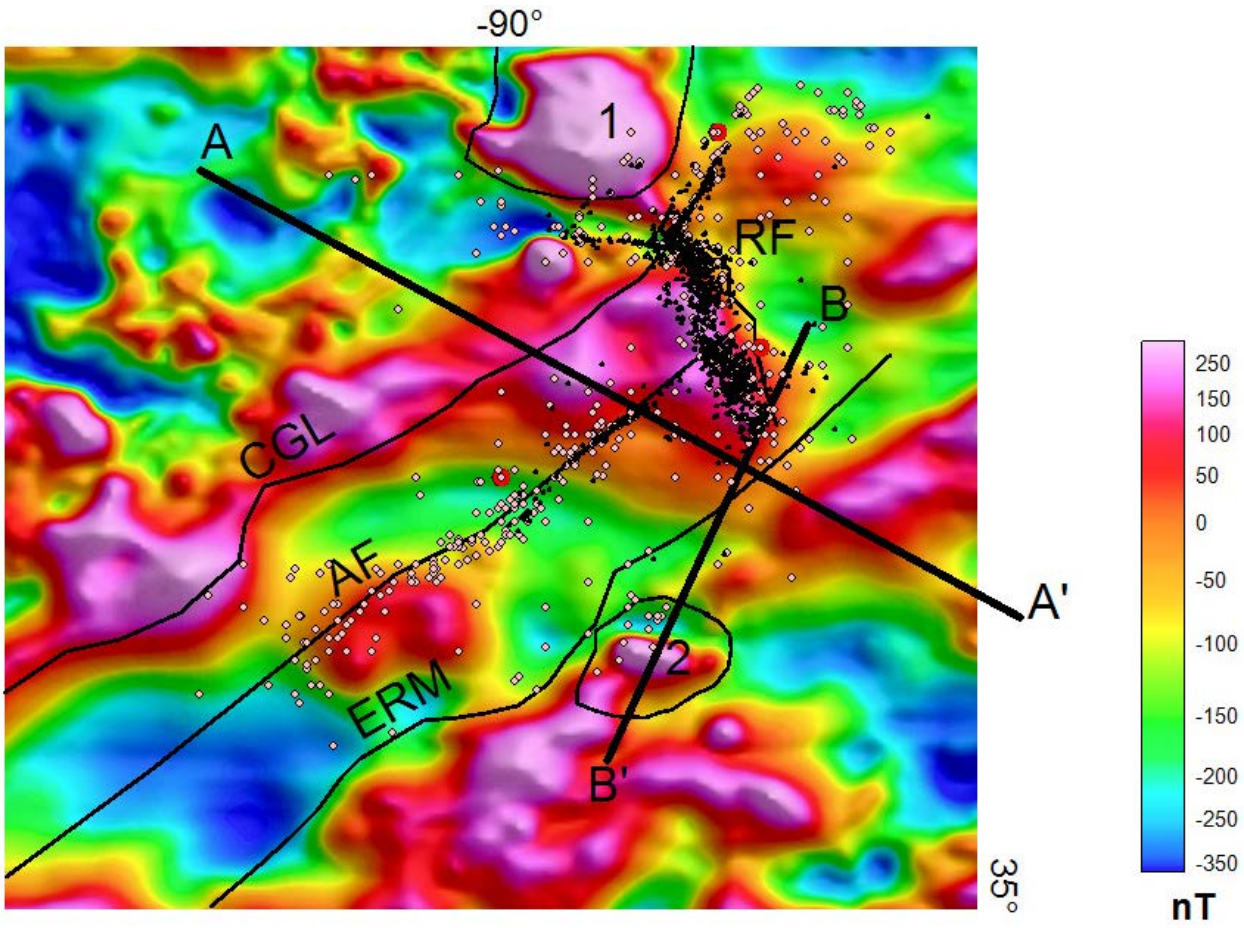

Fig. 9. Total magnetic field anomaly map of study area reduced to pole. Data from North America Magnetic Data (USGS database). The CGL and ERM appear as prominent northeast-trending lineaments (solid lines). The Bloomfield (1) and Covington (2) plutons are associated with semi-circular magnetic highs due to high susceptibility of mafic to ultramafic minerals. Lineations formed by high magnetic gradients are believed to be associated with faults that juxtapose differing rock types. Seismicity is concentrated along the margins of the Bloomfield pluton, within the magnetic high along RF, and linearly along AF. Although the Missouri batholith forms a circular anomaly in the gravity data, its expression in the magnetic data is not apparent.

the magnetic highs, which are interpreted as smaller intrusive bodies. Although the Missouri batholith forms a large circular anomaly in the gravity data, its expression in the magnetic data is not clearly apparent (Figure 9).

Filtering and Wavelength Separation

The TDR was used to show the spatial extent of the causative bodies in the gravity data (Figure 10). The zero contour line on the tilt derivative map is inferred to reflect the shape of the sources for the gravity anomalies. The resulting map suggests that the Covington pluton is part of a much larger complex that extends into the central portion of the rift, near the central axis. From this map, the Covington pluton extends through the central portion of the rift, as first proposed by Hildenbrand et al. (2001). There appears to be a slight association between the zero contour and some of the earthquake epicenters, but not all.

Figure 11 contains the result of calculating the tilt derivative for the total field anomaly map. Also plotted are interpreted faults from Csontos et al. (2008) to compare the location of prominent lineations in the map with the locations from their basement mapping. Although this overlay shows that many of the magnetic lineations line up with the proposed fault locations, some of the lineations extend beyond the mapped faults.

Like the TDR, the SVD of the gravity data can be used to enhance the understanding of key geologic features (Figure 12). The RF is shown to cross both to the CGL and ERM, although the CGL and ERM are less pronounced in this anomaly map. The size and shape of both the Bloomfield and Covington plutons in the SVD are very similar to that seen in the TDR zero contour. However, there is a small offset in the anomaly associated with the Covington pluton.

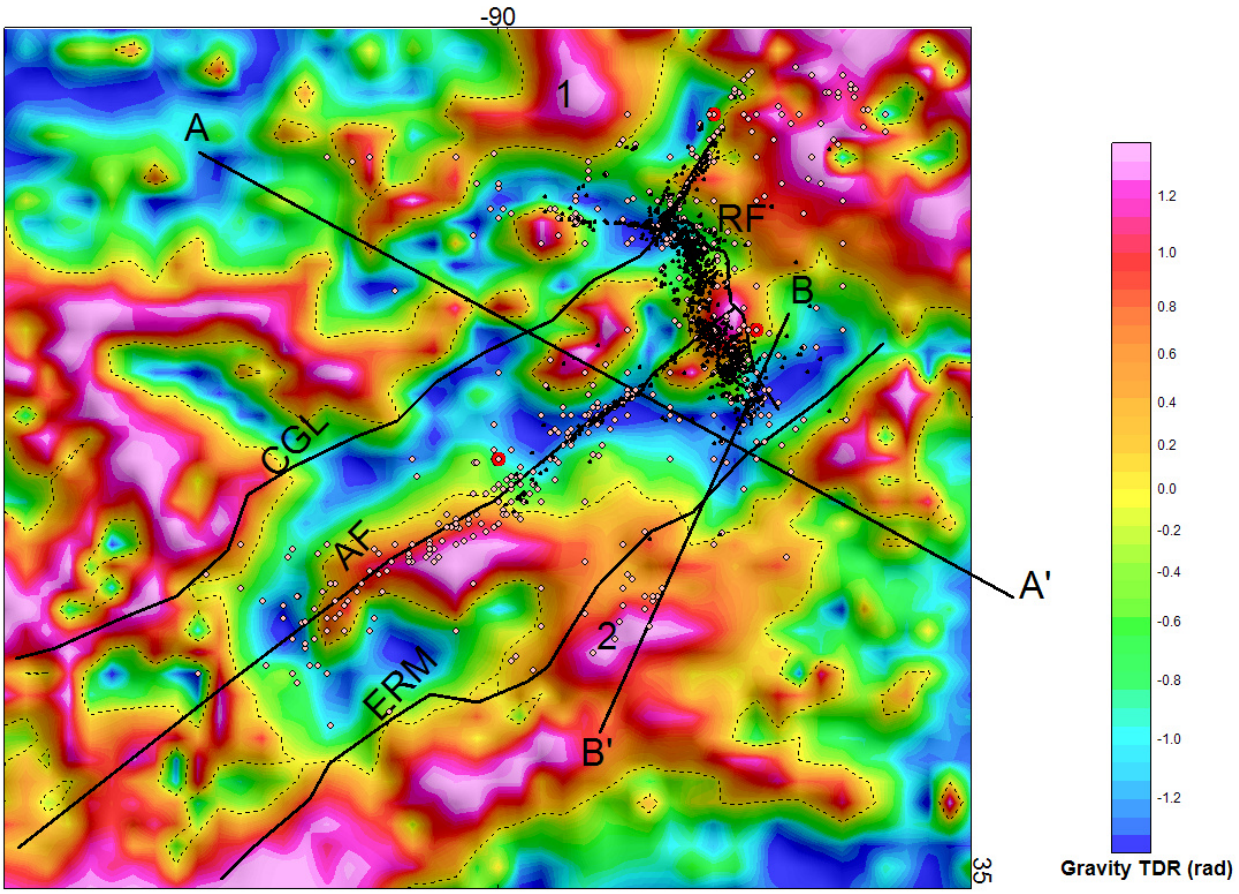

Fig. 10. Tilt derivative of the Bouguer anomaly map. The zero contour is plotted as a thin black line. The earthquake epicenters appear to close to the zero contour only in some areas.

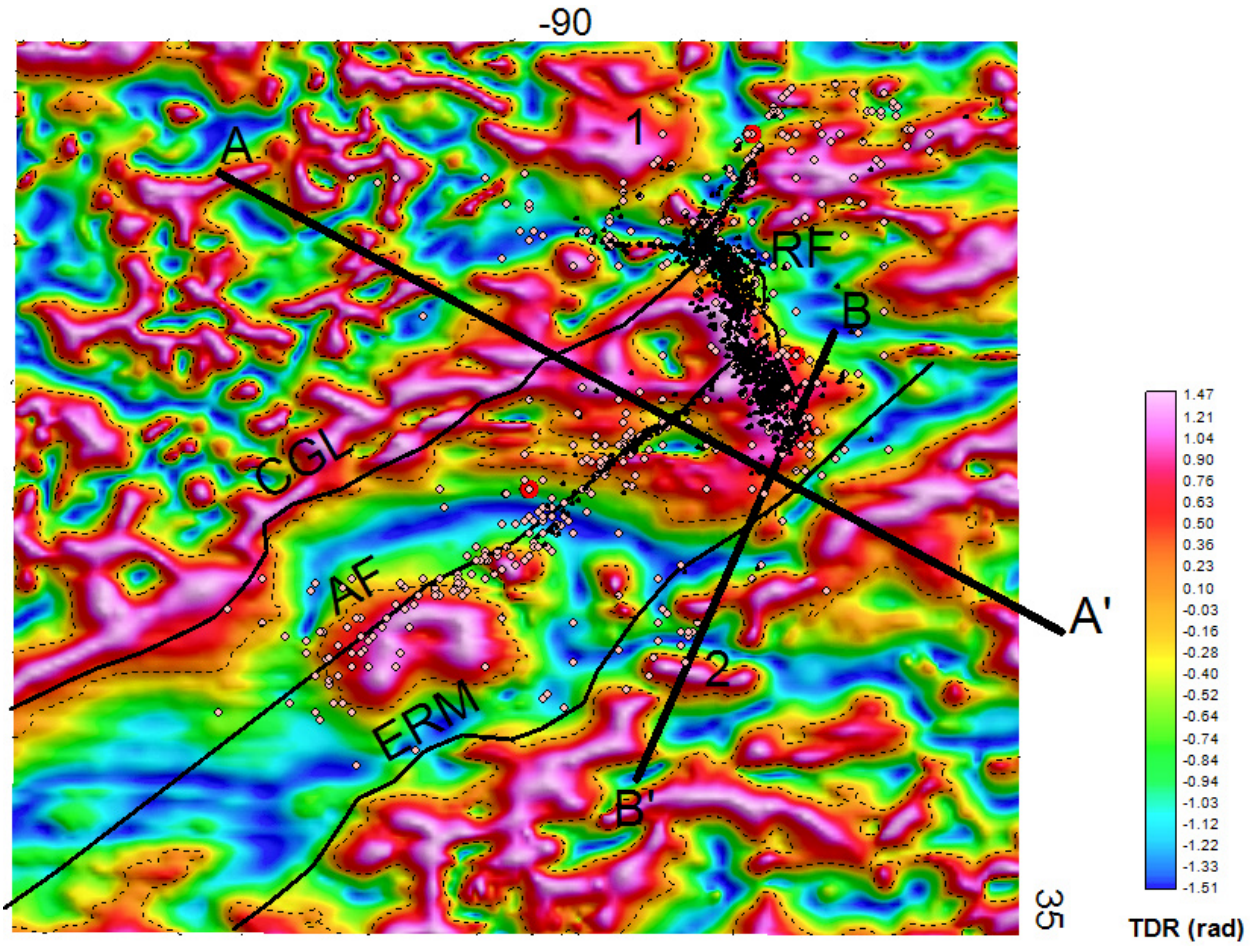

Fig. 11. Magnetic tilt derivative (TDR) applied to the TFA data. The zero contour is plotted as a dashed black line. Some proposed fault locations (black lines) from Csontos et al. (2008) are closely correlated with some lineations in the TDR (e.g., Axial fault=AF, CGL=Commerce Geophysical Lineament, ERM=Eastern Rift Margin, and Reelfoot fault=RF.

The SVD of the total field magnetic data (Figure 13) has limited utility for imaging smaller geologic structures. It does, however, show the margins of the rift as clear lineaments bordering the area containing the thick sediments of the central rift. Neither the Bloomfield nor the Covington plutons appear as distinct anomalies in this filtered map.

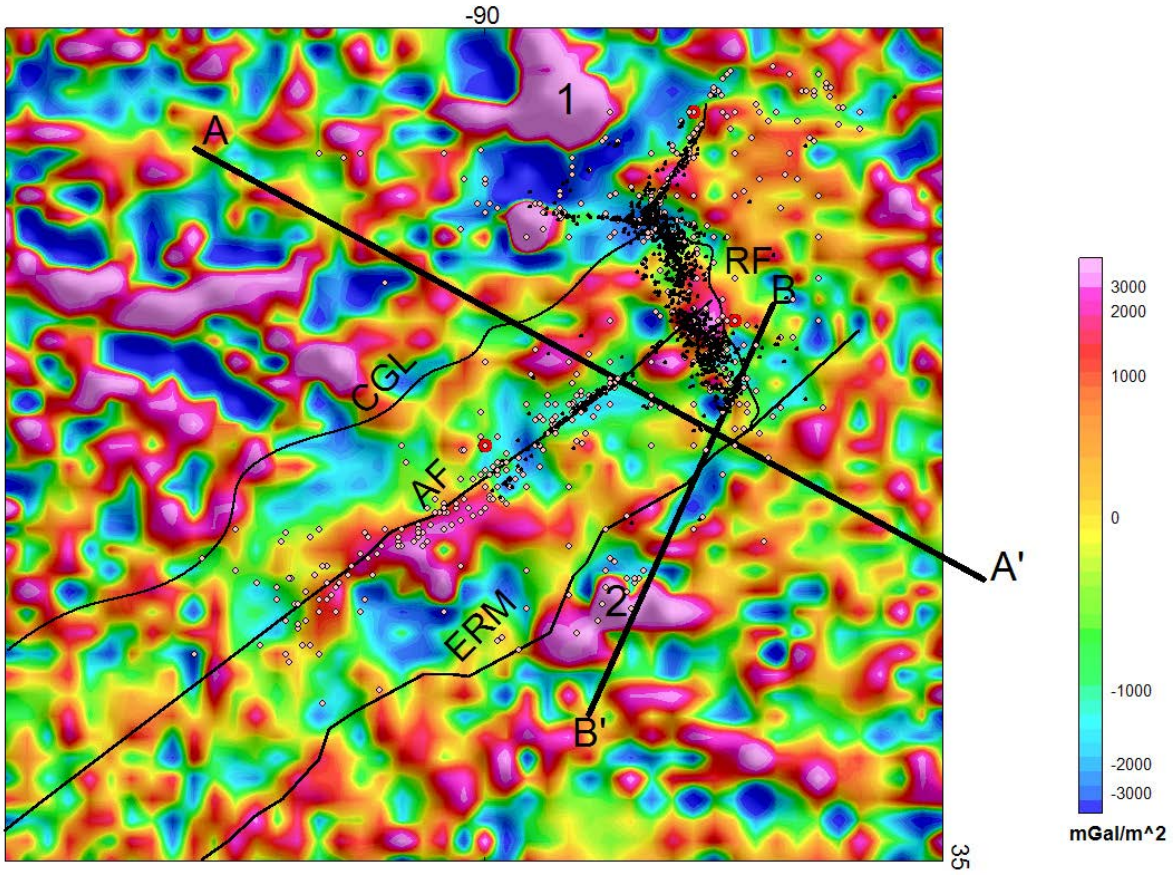

Fig. 12. SVD of the complete Bouguer gravity anomaly data. This map shows RF as crossing both the CGL and ERM. The expression of the Bloomfield Pluton (1) and Covington Pluton (2) is similar to that defined by the zero contour in the TDR map (Fig. 10)

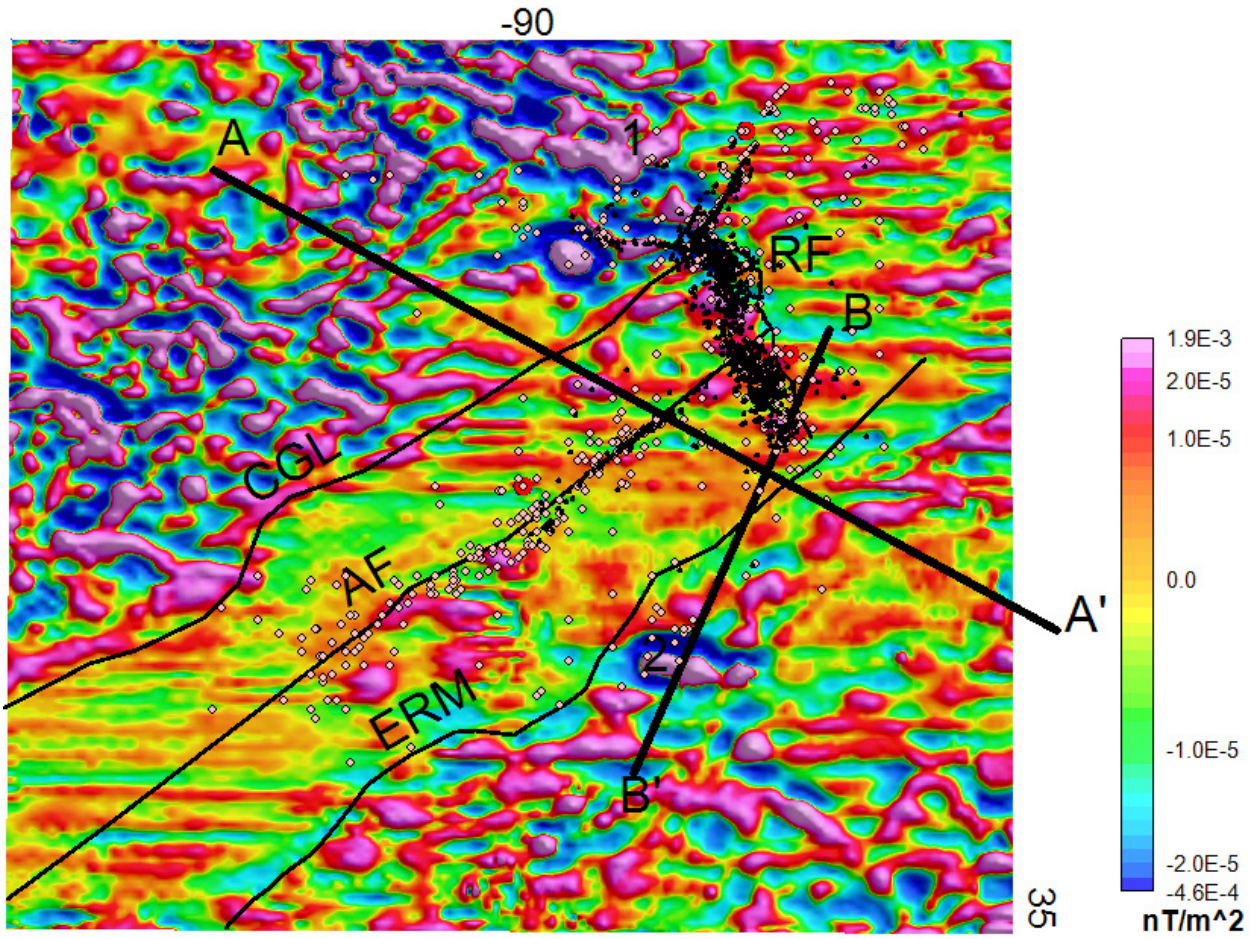

Fig. 13. SVD of the total magnetic field anomaly data. High values are along the CGL and ERM define the extent of the Reelfoot rift graben. Scattered highs within the central rift likely correlate with plutons of varying composition. Neither the Bloomfield nor Covington plutons are delineated in this filtering technique. Horizontal lines are an artifact of the processing

Profile Models

The gravity and magnetic profiles (A-A′ and B-B′) modeled in this study were chosen to cross prominent features in the gravity and magnetic data including the rift margins, the Reelfoot fault, and the Covington pluton (Figures 8 and 9). Line A-A′ is approximately 200 km in length and oriented perpendicular to the rift margins. Line B-B′ intersects A-A′ and is approximately 100 km in length, oriented subparallel to the strike of the Reelfoot graben. Together, the profiles give a pseudo-3D representation of the overall structure of the study area.

The densities and magnetic susceptibilities of the geologic units are expressed by polygons in the cross-section. All cross-sections extend to a depth of 60 km below the surface. The resulting best-fit models are consistent with other published models in nearby areas (Mooney et al., 1983; Hildenbrand, 1985; Liu et al., 2017).

Profile A-A′

Gravity data along profile A-A′ follow a regional trend ranging from a low of approximately -35 mGal in the northwestern section of the profile to high of about -10 mGal at about 150 km along the transect (Figure 14, middle panel). Two local highs in the gravity data occur at ~ 90 km and ~150 km along the profile. The magnetic data curve (Figure 14, upper panel) shows much shorter wavelength variations, with a range extending from ~ -300 nT to ~ 300 nT. A large magnetic high occurs at ~80 km.

The best-fit model for profile A-A′ indicates a crustal thickness of ~ 42 km. A high-density body (3150 kg/m^3; 0 SI), referred to as a "rift pillow" in earlier work, lies directly above the mantle and floors the Reelfoot rift. To either side, the lower crust is modeled with a density of 2920 kg/m^3 and a magnetic susceptibility ranging from 0.035 SI to 0.041 SI. A large body,

interpreted as a mafic intrusion (2830 kg/m^3; 0.063 SI), crosscuts the lower crust. The structure of the intrusion has two depressions which coincide with the rift (see discussion). Where the profile crosses the central rift, both the mafic intrusion and rift pillow show structural depressions.

The mafic body in the central part of the profile intrudes Precambrian rocks (2720 kg/m^3; 0.063 SI) in the upper crustal layer. Overlying the Precambrian rocks are a series of polygons representing plutonic rocks of varying densities and susceptibilities. Two main groups of intrusive rocks are indicated (colored white or green). The white bodies are associated with short wavelength magnetic anomalies and decreasing gravity values. These bodies (1-8) have uniform densities of 2720 kg/m^3 but varying susceptibilities, ranging from 0 to 0.033 SI. They are located outside of the western boundary of the rift and have a different lithology from those within the rift. The green units (A-F) extend through the rift and persist east of the ERM. These units are interpreted as dense mafic intrusives. Sharp contrasts in density and susceptibility values at the contacts among them suggest mineral fractionation or varying magmatic sources (see discussion). Intrusive rocks in the cross-section are overlain by a thin, low-density layer (2663 kg/m^3; 0.0 SI) that begins and ends at the approximate rift boundaries. This layer correlates to the low-velocity layer seen in models derived from seismic refraction data (Mooney et al., 1983). Paleozoic rocks (2690 kg/m^3; 0.0 SI) and Quaternary rocks (2200 kg/m^3; 0.0 SI) that constitute the basin fill make up the remainder of the model.

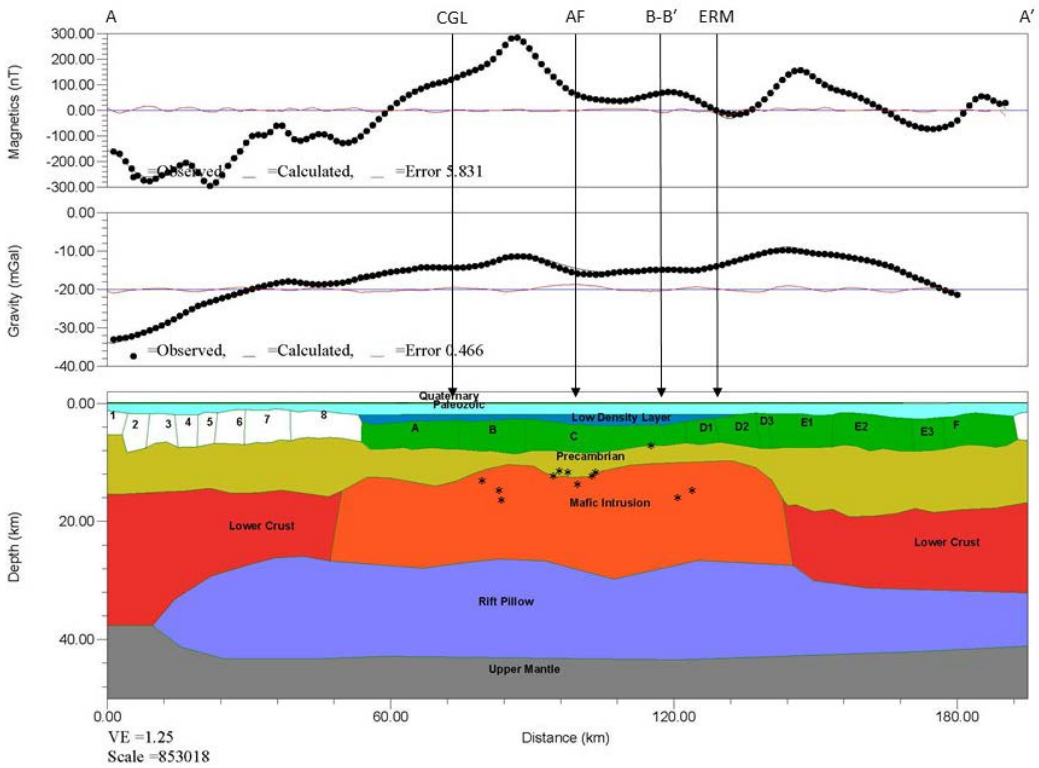

Fig. 14. Profile A-A′ crosses the CGL, AF, B-B′, and ERM. (See Figs. 1, 8, 9 for locations). Stars represent approximate earthquake hypocenters. Best-fit model is consistent with previously proposed nearby models (e.g., Mooney et al., 1983; Hildenbrand 1985; and Liu et al., 2017). Units were modeled using density and susceptibility values shown in Table 1. Key features of the model are the high-density rift pillow and large mafic intrusion in the central portion of the cross-section, located in the Reelfoot graben. Plutonic rocks in the upper crust are separated into two groups: mafic, high-density/high-susceptibility rocks (green polygons) and intermediate to felsic, high-density/lower susceptibility rocks (white polygons). Short wavelength variations in the magnetic data curve reflect variations in magnetic susceptibilities.

Unit Symbol	Depth Range (km)	Modeled Density (kg/m^3)	Susceptibility (SI)
Quaternary	0.0 – 0.05	2200	0
Paleozoic	0.05 – 2.0	2690	0
Low Density	2.0 – 3.9	2663	0
Precambrian	5.0 – 15.0	2720	0.063
Lower Crust	15.0 – 38.0	2920	0.035 / 0.041
Mafic Intrusion	10.0 – 28.0	2830	0.063
Rift Pillow	26.0 – 42.0	3150	0
Upper Mantle	37.0 – 50.0	3310	0
1 to 8	2.0 – 7.0	2720	0.0-0.033
A	3.2 – 7.8	2800	0.088
B	3.0 – 8.5	2780	0.097
C	3.1 – 8.3	2800	0.079
D1-D3	2.0 - 8.0	2770	0.044-0.052
E1-E3	2.0 – 8.0	2840	0.039-0.059
F	2.1 – 7.4	2770	0.038

Table 1. Polygons within cross-section model (Figure 14) for profile A-A′, with corresponding geologic interpretation. Listed are depth ranges, density, and susceptibility for each unit. Colors match units shown in Fig. 15.

Profile B-B′

Gravity data show a steady trend that increases from approximately -15 m/Gal in the north to a high anomaly of ~ 30 m/Gal in the south (Figure 15). As in profile A-A′, the magnetic data show more variations in an overall trend. The range of the magnetic data is from ~ -175 nT in the north and central portions of the model to a high anomaly of ~ 450 nT that aligns closely with a broad high in the gravity data curve. An inflection point and relative maximum are observable in the northern portion of the profile where it approaches and crosses the extension of the RF. As the profile continues to the south and crosses the location of ERM, the curve exhibits a localized high bracketed by two minimum values. The two peaks in the magnetic and gravity profiles, respectively, line up with the location of the Covington pluton, suggesting that this body has a dense magnetic core; however, short-wavelength undulations in the magnetic data curve suggest that its magnetic susceptibility is variable.

The lowest two layers in the model represent the upper mantle and rift pillow (see A-A′ for description). At the contact of the lower crust (2920 kg/m^3) (0.035 SI) with the large mafic intrusion (2830 kg/m^3) (0.063), the profile crosses RF. The model suggests that seismicity associated with the RF has a strong correlation with this contact. Precambrian rocks with density 2720 kg/m^3 and susceptibility 0.063 SI overlie the lower crust and mafic intrusion. A thinning of this unit occurs to the south of the contact between the lower crust and mafic intrusion. Units labelled 1-6, with varying densities (2710 – 2790 kg/m^3 and susceptibilities (0.018-0.09), extend from the northern portion of the model and end in close proximity to the ERM. Units C1 - C8 have densities varying from 2770 to 2950 kg/m^3 and susceptibilities from 0.028 to 0.118 SI. These encompass intrusive rocks associated with and surrounding the Covington pluton. The highest values for magnetic susceptibility and density occur directly over the Covington pluton.

The upper portion of the model consists of a low density unit directly above the plutonic rocks represented by polygons 2 through 6. Above these, Paleozoic rocks (2690 kg/m^3) and Quaternary rocks (2200 kg/m^3) make up the remainder of the model.

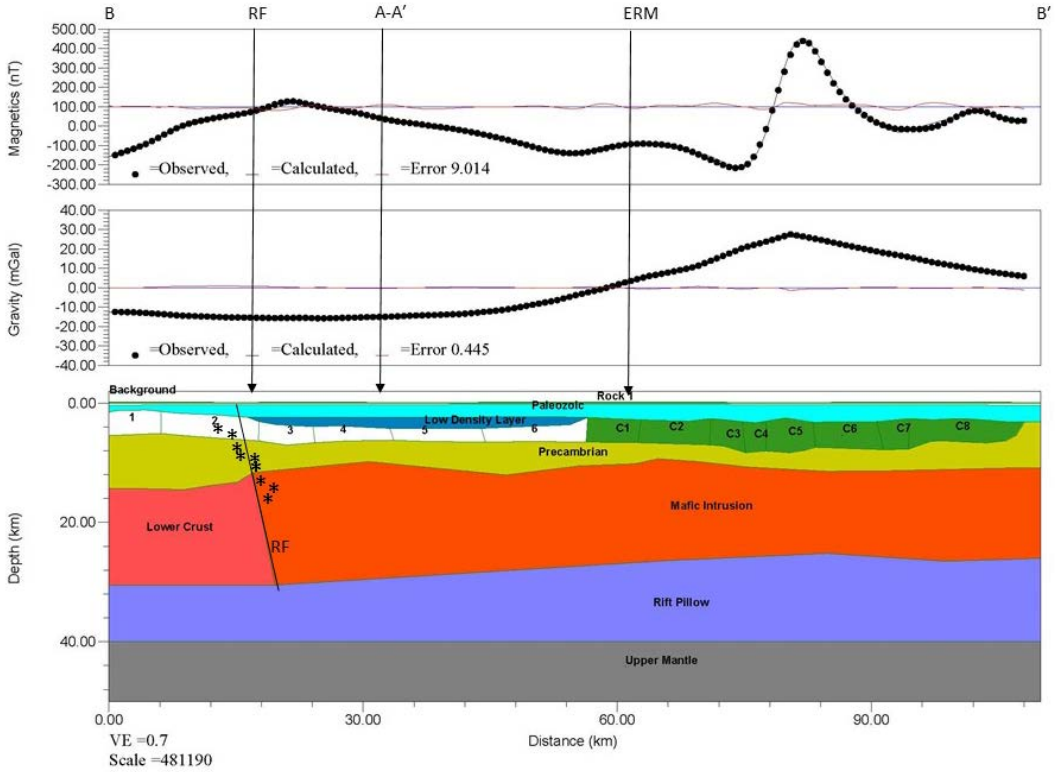

Fig. 15. Profile B-B′ crosses the RF, profile A-A′, and the ERM (see Figs 1, 8, 9 for locations). Stars show approximate earthquake hypocenters. The model is consistent with previous interpretations of profiles located in the same general area (e.g., Mooney et al. 1983; Hildenbrand, 1985; and Liu et al., 2017). Units were modeled using density and susceptibility values shown in Table 2.

Unit Symbol	Depth Range (km)	Modeled Density (SI)	Susceptibility (SI)
Quaternary	0.0 – 0.05	2200	0
Paleozoic	0.05 – 2.0	2690	0
Low Density	2.0 – 3.9	2663	0
Precambrian	5.0 – 15.0	2720	0.063
Lower Crust	15.0 – 30.0	2920	0.035
Mafic Intrusion	10.0 – 28.0	2830	0.063
Rift Pillow	26.0 – 42.0	3150	0
Upper Mantle	37.0 – 50.0	3310	0
1 to 6	3.0-7.0	2710 - 2790	0.018-0.09
C1 - C8	2.5 – 7.0	2770 - 2950	0.028 - 0.118

Table 2. List of model blocks and their depth ranges, density, and susceptibility for profile B-B′. Colors match those in the cross-sectional model (Fig. 15).

Discussion

The models presented in this study are consistent with those done previously in the NMSZ and have allowed for an enhanced understanding of the relationship to the subsurface structure to the observed seismicity in the region. They have also provided insight into the geologic evolution of the central U. S. Potential field maps of gravity and magnetic data produced in this study add clarity to prominent features that were previously identified (e.g., Mooney, 1983; Hildenbrand, 1985). For instance, the expression of the Bloomfield and Covington plutons in the complete Bouguer gravity and total field magnetic anomaly maps indicates that these bodies are composed of dense, highly magnetic rocks compared to the surrounding rocks (Figure 8 and 9). When filtering techniques were applied to the potential fields, however, the dimensions of the Covington pluton changed significantly, suggesting that this intrusion is not uniform in composition (Figures 10, 11, 12, and 13). The cross-sectional models produced in the study are consistent with this interpretation in that the data are best fit by introducing two distinct groups of bodies in the upper crust to represent rocks of variable magnetic susceptibilities (Figures 14 and 15). This change in the physical properties of the rocks would seem to suggest that they either were formed from different magmatic events or through fractionation cooling.

The maps and models derived in this study also lend some insight into the relationship of seismicity in the central U.S. to the subsurface structure. Earthquakes in the NMSZ align in three major orientations: a northeast-trending group aligned along the AF, a northwest-trending band that defines the RF, and a second but shorter northeast-trending band aligned along the northern

extension of the CGL, to the southeast of the Bloomfield pluton. Profile A-A′ crosses the group of earthquakes distributed along AF (Figure 1). The epicenters for this band of seismicity are situated in the middle of the model along profile A-A′, directly above the large mafic intrusion (Figure 14). In this portion of the model, the top of the body representing the intrusion is structurally higher than the less dense surrounding host rocks in the upper crust, which might serve to concentrate stress in the central portion of the NMSZ. This, as well as the contrast of the rift pillow and intrusive bodies, might provide a mechanism for the linear distribution of the earthquakes along the AF axis. Profile B-B′ crosses the RF at a location directly above the contact between the mafic intrusion and lower crust in the model, again suggesting that this large mafic body exerts some control on the earthquakes associated with the RF. Dunn et al. (2013), in their relocation of NMSZ earthquakes, show hypocentral depths of most seismicity between 5 and 15 km, which is the same modeled depth of the mafic intrusion in both profiles.

Although the results of this study suggest that the large intrusive body beneath the central NMSZ is influencing the local stress regime, which may in turn explain its connection to the seismicity, the kinematics of the intrusion relative to other forces acting on the zone (e.g., far-field plate boundary stresses) are not clear. Liu et al. (2017) proposed that the density associated with the mafic intrusion is causing isostatic adjustment, which began after its emplacement. This idea builds on a model by Pollitz et al. (2001), who asserts that an excess mafic body underneath the rift would exert a primary downward pull on the upper crust, leading to primary thrust faulting and secondary strike-slip faulting. However, based on his global positioning survey data, Newman et al. (1999) claimed that there was little to no evidence for strain accumulation across the NMSZ, a result that makes the mechanism of the sinking body somewhat problematic. If isostatic adjustment is the mechanism behind seismicity in the NMSZ, then the excess mass is

likely resulting from contrast in density between the mafic intrusion and the Precambrian rocks of the upper crust, in addition to the overlying thick sequence of sediments in the central embayment.

As revealed in the models presented here, the present-day crustal structure in the NMSZ is the result of a series of tectonic events that served to modify and shape the lithosphere. Lithospheric extension, normal faulting, and formation of the rift pillow at the base of the crust is consistent with other global examples of rift zones (Mooney et al., 1983) and is represented by the units forming the lower crust in the models. Although excess heat and depleted mantle may have initially caused uplift of the central rift, far-field compressional forces acting on the plate boundary to the east initiated subsidence and basin formation in the newly formed rift zone. The introduction of the inland seaway allowed for the deposition of Paleozoic marine sediments, represented by the units in the upper 4 km of the models. The models proposed here are consistent with the assertion of Cox and Van Arsdale (2002) that propose the passage of the Bermuda hot spot beneath the NMSZ in Early to Mid-Cretaceous, leading to uplift and reactivation of Precambrian faults, followed by formation of a large mafic intrusion in the lower crust and a series of intrusions in the upper crust as mantle material traveled along conduits formed by the fault planes. The contrast in magnetic susceptibilities between the upper crustal plutons in the model suggest variable compositions and may reflect magmatic fractionalization or staggered periods of magmatic injections. Although isostatic adjustment may play a role in the mechanism for seismicity in the NMSZ today, the region shows little evidence of strain accumulation based on GPS studies. The spatial correlation between the large mafic intrusive body in the lower crust and the present day seismicity suggests, however, that the intrusion may have an influence on the stress regime. Future work to understand the kinematics, petrology, and

geochronology of the intrusive bodies in the NMSZ will aid in refining the mechanisms for seismicity in the NMSZ.

Conclusions

The results of this study suggest possible structures that act to concentrate stresses in the NMSZ leading to the observed seismicity and provides insight into the tectonic origins of these structures. Potential field observations show that anomalies associated with igneous intrusions are concentrated along the rift margins, and the Reelfoot Fault. The seismicity occurs in three main orientations: along the AF, along the RF, and around the Bloomfield Pluton. Profile modeling shows that earthquakes occurring along the AF and the RF are spatially associated with the presence of a large mafic intrusion extending through the rift zone. The intrusions in the NMSZ are believed to be related to the passage of the Bermuda Hot Spot, which in turn led to reactivation of Precambrian faults in the NMSZ. Future work that would aid in the understanding of the findings of this study would be higher resolution potential field mapping and geochronological work to support or refute the timing and role of the Bermuda Hot Spot and its associated intrusions.

References

Blakely, R.J., Connard, G.G., and Curto, J.B., 2016, Tilt Derivative Made Easy: Geosoft Inc. Resources, https://www.geosoft.com/media/uploads/resources/tilt_derivative_made_easy_07-2016.pdf (accessed March 2019).

Braile, L. W., Hinze, W. J., Keller, G., Lidiak, E. G., & Sexton, J. L.,1986, Tectonic development of the New Madrid rift complex, Mississippi Embayment, North America: Tectonophysics, v. 131, p. 1-21. doi:10.1016/0040-1951(86)90265-9.

CEUS-SSC, 2015, GIS Database: http://www.ceus-ssc.com/Report/GIS.html (accessed June 2016).

Cox, R.T., and Van Arsdale, R.B., 2002, The Mississippi Embayment, North America: a first order continental structure generated by the Cretaceous superplume mantle event: Journal of Geodynamics, v. 34, p. 163–176, doi: 10.1016/s0264-3707(02)00019-4.

Cushing, E.M., Boswell, E.H., Hosman, R.L., General geology of the Mississippi Embayment: Water resources of the Mississippi Embayment, 1964, U.S. Geological Survey Professional Paper 448-B.

Csontos, R., & Van Arsdale, R.B.., 2008, New Madrid seismic zone fault geometry: Geosphere, v. 4, p. 802-813. doi:10.1130/ges00141.1.

Dunn, M., Deshon, H.R., and Powell, C.A., 2013, Imaging the New Madrid Seismic Zone using double-difference tomography: Journal of Geophysical Research: Solid Earth, v. 118, p. 5404–5416, doi: 10.1002/jgrb.50384.

Ervin, C.P., & McGinnis, L.D., 1975, Reelfoot rift – Reactivated precursor to the Mississippi Embayment: Geological Society of America Bulletin, v. 86, p. 1287-1295.

Hardesty, K., Wolf, L. W., & Bodin, P., 2010, Noise to signal: A microtremor study at liquefaction sites in the New Madrid Seismic Zone: Geophysics, v. 75, no. 3. doi:10.1190/1.337434.

Hildenbrand, T. G., 1985, Rift structure of the Northern Mississippi Embayment from the analysis of gravity and magnetic data: Journal of Geophysical Research, v. 90, no. B14, p. 12607-12622. doi:10.1029/jb090ib14p12607.

Hildenbrand, T. G., & Hendricks, J. D., 1995, Geophysical setting of the Reelfoot Rift and relations between rift structures and the New Madrid Seismic Zone: U.S. Geological Survey Professional Paper, 1538-e.

Hildenbrand, T., Stuart, W., and Talwani, P., 2001, Geologic structures related to New Madrid earthquakes near Memphis, Tennessee, based on gravity and magnetic interpretations: Engineering Geology, v. 62, p. 105–121, doi: 10.1016/s0013-7952(01)00056-4.

Langenheim, V., & Hildenbrand, T., 1997, Commerce geophysical lineament - Its source, geometry, and relation to the Reelfoot rift and New Madrid seismic zone: GSA Bulletin, v. 109, no. 5, p.580-595.

Liu, L., Gao, S. S., Liu, K. H., & Mickus, K., 2017, Receiver function and gravity constraints on crustal structure and vertical movements of the Upper Mississippi Embayment and Ozark Uplift: Journal of Geophysical Research: Solid Earth, v. 122, p. 4572-4583. doi:10.1002/2017jb014201.

Mooney, W., Andrews, M., Ginzburg, A., Peters, D., & Hamilton, R., 1983, Crustal structure of the Northern Mississippi Embayment and a comparison with other continental rift Zones: Tectonophysics, p. 327-348. doi:10.1016/b978-0-444-42198-2.50025-0.

Newman, A., Stein, S., Webber, J., Engeln, J., Mao, A., and Dixon, T., 1999, Slow deformation and lower seismic hazard at the New Madrid Seismic Zone: Science, v. 284, 619–621, doi: 10.1126/science.284.5414.619.

Pollitz, F.F., 2001, Sinking mafic body in a reactivated lower crust: A mechanism for stress concentration at the New Madrid Seismic Zone: Bulletin of the Seismological Society of America, v. 91, p. 1882–1897, doi: 10.1785/0120000277.

Pollitz, F.F., and Mooney, W.D., 2014, Seismic structure of the Central U.S. crust and shallow upper mantle: Uniqueness of the Reelfoot Rift: Earth and Planetary Science Letters, v. 402, p. 157–166, doi: 10.1016/j.epsl.2013.05.042.

Rabak, I., Langston, C., and Powell, C., 2011, The Reelfoot Magnetic Anomaly and its relationship to the Pascola Arch and the Reelfoot Fault: Seismological Research Letters, v. 82, p. 132–140, doi: 10.1785/gssrl.82.1.132.

Ravat, D., Braile, L., & W. H., 1987, Earthquakes and plutons in the midcontinent: Evidence from the Bloomfield Pluton New Madrid Rift Complex: Seismological Research Letters, v. 58 no. 2, p. 41-52.

Reynolds, J.M., 1997, An introduction to applied and environmental geophysics: Oxford, Wiley-Blackwell.

Tuttle, M. P., Schweig, E. S., Sims, J. D., Lafferty, R. H., Wolf, L. W., Haynes, M. L., 2002, The earthquake potential of the New Madrid seismic zone, Bulletin of the Seismological Society of America, v. 92, no. 6, p. 2080-2089.

U.S. Geological Survey, 2002, Digital data grids for the magnetic anomaly map of North America: https://pubs.usgs.gov/of/2002/ofr-02-414/ (accessed August 2017).

Verduzco, B., Fairhead, J.D., Green, C.M., and Mackenzie, C., 2004, New insights into magnetic derivatives for structural mapping: The Leading Edge, v. 23, p. 116–119, doi: 10.1190/1.1651454.

Zhan, Y., Gregg, P., Gregg, P., Hou, G., and Hou, G., 2016, Stress development in heterogenetic lithosphere: insights into earthquake processes in the New Madrid Seismic Zone: doi: 10.1130/abs/2016nc-275226.